AGU PUBLICATIONS

Geophysical Research Letters

RESEARCH LETTER

10.1002/2017GL074362

Key Points:

- Generation of discrete magnetosonic emissions with long-lasting (15-25 min) rising tones by substorm-injected hot protons
- Consistent frequency-time structures of magnetosonic emissions between locations separated by $\Delta L \leq 2.0$ and by ΔMLT ≤ 4.2
- Direct evidence for radial and azimuthal propagation of magnetosonic waves in the Van Allen radiation belts

Supporting Information:

- Supporting Information S1

Correspondence to:
Z. Su,
szpe@mail.ustc.edu.cn

Citation:
Su, Z., G. Wang, N. Liu, H. Zheng, Y. Wang, and S. Wang (2017), Direct observation of generation and propagation of magnetosonic waves following substorm injection, *Geophys. Res. Lett.*, *44*, 7587–7597, doi:10.1002/2017GL074362.

Received 30 MAY 2017
Accepted 13 JUL 2017
Accepted article online 18 JUL 2017
Published online 5 AUG 2017

Direct observation of generation and propagation of magnetosonic waves following substorm injection

Zhenpeng Su[1,2], Geng Wang[1,2,3], Nigang Liu[1,2,3], Huinan Zheng[1,2], Yuming Wang[1], and Shui Wang[1]

[1]CAS Key Laboratory of Geospace Environment, Department of Geophysics and Planetary Sciences, University of Science and Technology of China, Hefei, China, [2]Collaborative Innovation Center of Astronautical Science and Technology, University of Science and Technology of China, Hefei, China, [3]Mengcheng National Geophysical Observatory, School of Earth and Space Sciences, University of Science and Technology of China, Hefei, China

Abstract Magnetosonic whistler mode waves play an important role in the radiation belt electron dynamics. Previous theory has suggested that these waves are excited by the ring distributions of hot protons and can propagate radially and azimuthally over a broad spatial range. However, because of the challenging requirements on satellite locations and data processing techniques, this theory was difficult to validate directly. Here we present some experimental tests of the theory on the basis of Van Allen Probes observations of magnetosonic waves following substorm injections. At higher *L* shells with significant substorm injections, the discrete magnetosonic emission lines started approximately at the proton gyrofrequency harmonics, qualitatively consistent with the prediction of linear proton Bernstein mode instability. In the frequency-time spectrograms, these emission lines exhibited a clear rising tone characteristic with a long duration of 15–25 min, implying the additional contribution of other undiscovered mechanisms. Nearly at the same time, the magnetosonic waves arose at lower *L* shells without substorm injections. The wave signals at two different locations, separated by ΔL up to 2.0 and by ΔMLT up to 4.2, displayed the consistent frequency-time structures, strongly supporting the hypothesis about the radial and azimuthal propagation of magnetosonic waves.

1. Introduction

Magnetosonic waves are the low-frequency (a few to several hundreds of hertz) whistler mode emissions with magnetic compressibility $\sim>0.9$ confined near the magnetic equator [*Russell et al.*, 1970; *Gurnett*, 1976; *Santolík et al.*, 2002a; *Němec et al.*, 2005; *Tsurutani et al.*, 2014; *Balikhin et al.*, 2015]. These waves can occur over a broad range of radial distances and magnetic local times both inside and outside the plasmasphere [e.g., *Meredith et al.*, 2008; *Ma et al.*, 2013; *Shprits et al.*, 2013; *Hrbáčková et al.*, 2015]. Recently, magnetosonic waves have received increasing attention because of their potential importance in the radiation belt electron dynamics. Through the Landau resonance, magnetosonic waves can locally accelerate energetic electrons mirroring off the equator [*Horne et al.*, 2007] and produce the electron butterfly pitch angle distributions in the outer radiation belt [*Xiao et al.*, 2015] and the slot region [*Zhao et al.*, 2014; *Li et al.*, 2016; *Yang et al.*, 2017]. Through the bounce resonance [*Roberts and Schulz*, 1968], magnetosonic waves may remove the equatorially trapped energetic electrons [*Shprits*, 2009; *Chen et al.*, 2015]. Because of the latitudinal confinement of magnetosonic waves, the scattering of energetic electrons can arise even in the nonresonant regime [*Bortnik and Thorne*, 2010].

The ring distributions of protons around 10 keV have been suggested to provide the free energy for magnetosonic waves [e.g., *Gulelmi et al.*, 1975; *Perraut et al.*, 1982; *Boardsen et al.*, 1992; *Chen et al.*, 2010]. The corresponding Bernstein mode instability tends to generate magnetosonic waves at frequencies close to the harmonics of the proton gyrofrequency with wave vectors nearly perpendicular to the background magnetic field [*Curtis and Wu*, 1979; *Boardsen et al.*, 1992; *Horne et al.*, 2000; *Gary et al.*, 2010; *Liu et al.*, 2011]. Previous observations have shown that the magnetosonic emission lines can considerably deviate from the harmonics of the local proton gyrofrequency [*Santolík et al.*, 2002a, 2016] and even extend below the local proton gyrofrequency in the radiation belt slot region [e.g., *Li et al.*, 2016; *Yang et al.*, 2017]. These discrepancies may be interpreted as a result of the magnetosonic wave propagation [*Kasahara et al.*, 1994; *Horne et al.*, 2000; *Chen and Thorne*, 2012; *Ma et al.*, 2014; *Santolík et al.*, 2016; *Horne and Miyoshi*, 2016]. However, it is challenging to directly validate this hypothesis because of the stringent requirements on satellite observations and data processing techniques. Simultaneous observations of magnetosonic waves by at least two satellites near the magnetic equator are required: one located around the wave source and the other located on the wave propagation path. *Boardsen et al.* [2014] showed the simultaneous observations of magnetosonic waves inside and outside the plasmasphere, albeit with a low resolution in frequency. Frequency resolution that resolves the harmonic structures is highly desirable when intercomparing emissions between different satellites.

In this letter, we show some experimental tests of the previous theory for magnetosonic wave generation and propagation in the Van Allen radiation belts. The required experimental situation was achieved by the Van Allen Probes mission [*Mauk et al.*, 2013], and the high-resolution frequency-time characteristic served as a good reference material for estimating the correlation between magnetosonic waves at different locations.

2. Data and Method

The Van Allen Probes mission consists of two identically instrumented spacecraft to explore the radiation belts surrounding the Earth [*Mauk et al.*, 2013]. The slight difference in the low inclination orbits of twin Van Allen Probes leads to the quasiperiodic variation in their spatial separation from ~0.1 to 5 R_E (Earth radii), allowing the experimental tests of the previous theory for magnetosonic wave generation and propagation around the equator. The data sets used here were collected by the Electric and Magnetic Field Instrument Suite and Integrated Science (EMFISIS) [*Kletzing et al.*, 2013], the Electric Field and Wave (EFW) instrument [*Wygant et al.*, 2013], and the Energetic Particle, Composition and Thermal Plasma Suite (ECT) [*Spence et al.*, 2013].

The local electric field $\mathbf{E}$ with a time resolution of ~11 s in the modified geocentric solar ecliptic coordinate system [*Wygant et al.*, 2013] was observed by the EFW instrument. The local magnetic field $\mathbf{B}_o$ with a time resolution of 1/64 s was detected by the triaxial fluxgate magnetometer (MAG) of the EMFISIS suite, and the corresponding equatorial magnetic field is estimated as $B_e = B_o B_{Me}/B_{Mo}$ with the TS04-modeled [*Tsyganenko and Sitnov*, 2005] ratio B_{Me}/B_{Mo} between equatorial and local magnetic field strengthes. The wave spectral matrix with a time resolution of ~6 s at frequencies from 5 Hz to 3 kHz is obtained as a subset of survey data of the waveform receiver (WFR) of the EMFISIS Waves instrument. The wave spectral matrix at frequencies 0–32 Hz is obtained through the fast Fourier transform (FFT) of the magnetic field data: (1) a 1024-point FFT with a time resolution of 16 s and a frequency resolution of 1/16 Hz for event overview and (2) a 4096-point 78% overlapped FFT with a time resolution of ~14 s and a frequency resolution of 1/64 Hz for intercomparing signals between different locations. The singular value decomposition method [*Santolík et al.*, 2003] is used to determine the wave vector direction and the planarity and ellipticity of wave polarization [*Santolík et al.*, 2002b]. The Poynting vector is calculated from the components of spectral matrices using a method of *Santolík et al.* [2010]. The local electron density N_e was measured by the high-frequency receiver [*Kurth et al.*, 2014] of the EMFISIS Waves instrument. The hot proton flux j was observed by the Helium, Oxygen, Proton, and Electron [*Funsten et al.*, 2013] and the Magnetic Electron Ion Spectrometer [*Blake et al.*, 2013] of the ECT suite. The corresponding phase space density (PSD) $F(v_\perp, v_\parallel) = j/p^2 = \sum_{i=1}^{N} F_i$ is modeled as a sum of bi-Maxwellian components

$$F_i = \frac{n_i}{\alpha_i(\sqrt{\pi}V_i)^3} \exp\left[-\frac{v_\parallel^2}{V_i^2} - \frac{v_\perp^2}{\alpha_i V_i^2}\right] \tag{1}$$

characterized by the density n_i, the thermal velocity $V_i = \sqrt{2T_i/m_p}$, and the loss-cone parameter α_i. The local plasma instability is analyzed by solving the full hot electromagnetic dispersion relation $D(\mathbf{k}, \omega) = 0$ [see *Horne*, 1989, equations (13)–(18)]. For a given wave frequency $\omega = 2\pi f$, a complex wave vector $\mathbf{k} = \mathbf{k_r} + i\mathbf{k_i}$ is found through the iteration. The convective growth rate is defined as $\boldsymbol{K_i} = -\mathbf{k_i} \cdot \mathbf{V_g}/|\mathbf{V_g}|$ with the wave group velocity $\mathbf{V_g}$.

3. Event on 21 August 2013

3.1. Overview

In Figure 1, we give an overview of the magnetosonic wave event on 21 August 2013. In the time range from 04:30 UT to 09:30 UT, Van Allen Probes were always in the high-density ($N_e > 100$ cm^{-3}) plasmasphere.

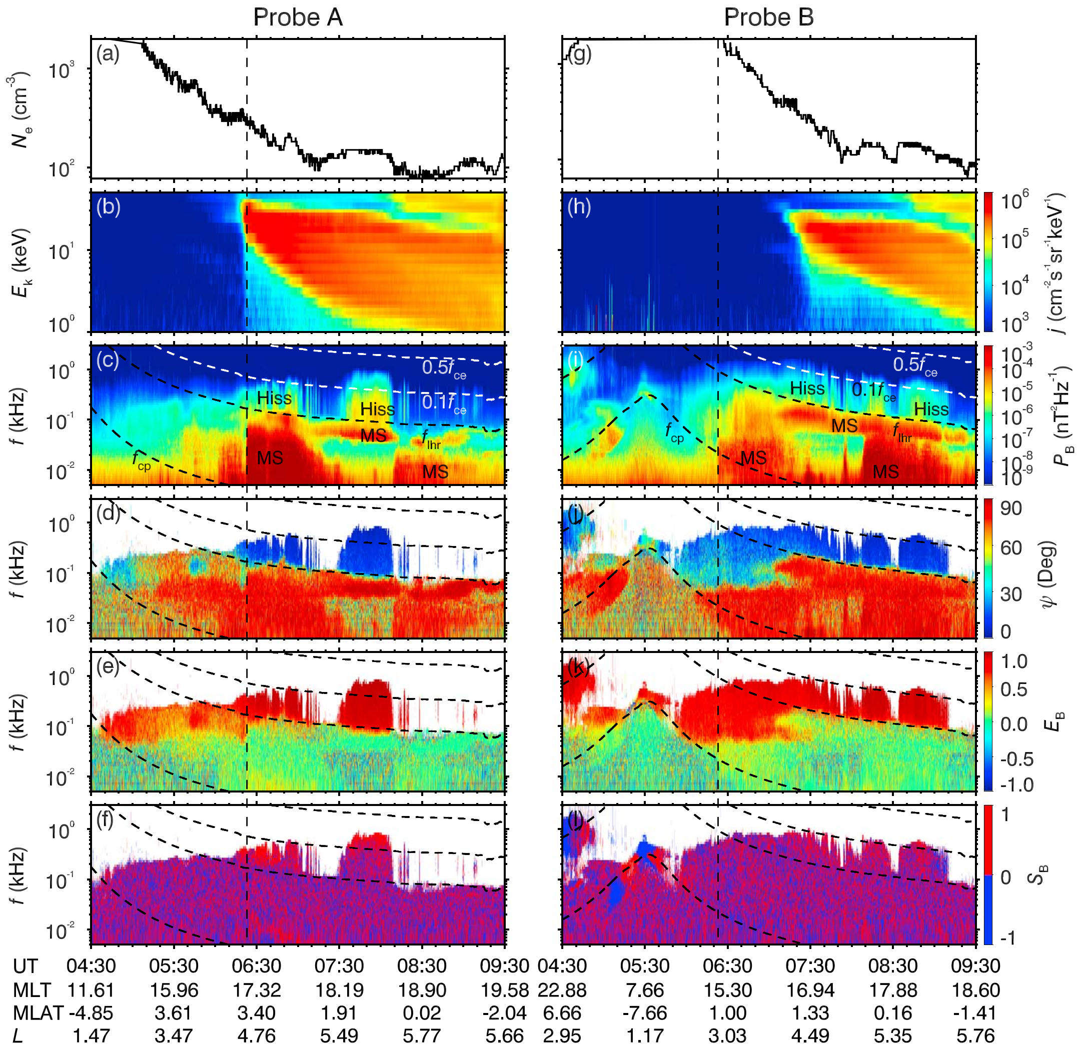

Figure 1. Generation and propagation of magnetosonic waves at frequencies above 5 Hz on 21 August 2013: (a, g) background electron density N_e, (b, h) spin-averaged proton flux j, (c, i) wave power spectral density P_B, (d, j) wave normal angle ψ, (e, k) wave ellipticity E_B (negative for left hand polarized waves and positive for right-handed ones), and (f, l) sign of field-aligned component of Poynting flux S_B (positive for parallel orientation and negative for antiparallel orientation).

After 06:00 UT, both probes were located in the duskside (15 < MLT < 20) equatorial (|MLAT| < 4°) region, conducive to the simultaneous detection of magnetosonic waves. Probe A experienced a substorm injection of hot protons with energies around 20 keV at 06:23 UT ($L = 4.6$ and MLT = 17.2). The substorm injection appeared to be wedge shaped in the energy-time spectrum. As observed by the WFR of Probe A, this substorm injection directly caused a prompt enhancement of magnetosonic waves (with ellipticity $E_B \approx 0$, normal angle close to $\psi \approx 90°$ and Poynting vector with a significant perpendicular component) below the lower hybrid resonant frequency f_{lhr}. Nearly at the same time, Probe B observed the emergence of magnetosonic waves around $L = 2.8$ and MLT = 15.1 in the absence of substorm injection. These magnetosonic waves in the radiation belt slot region extended obviously below the local proton frequency $f_{cp} = 20$ Hz and had approximately 10 times smaller intensities than those in the outer radiation belt. About 50 min later, Probe B encountered the substorm injection front at $L = 3.9$ and MLT = 16.5. These observations imply that the enhanced magnetosonic waves following the substorm injection were generated in the outer radiation belt (at least outside $L = 3.9$) and then propagated down to the slot region.

In the low-frequency range, the onboard spectra of WFR had a quite low resolution in frequency. To identify the wave frequency-time characteristics, we plot the FFT spectra of MAG fields of twin Van Allen Probes in

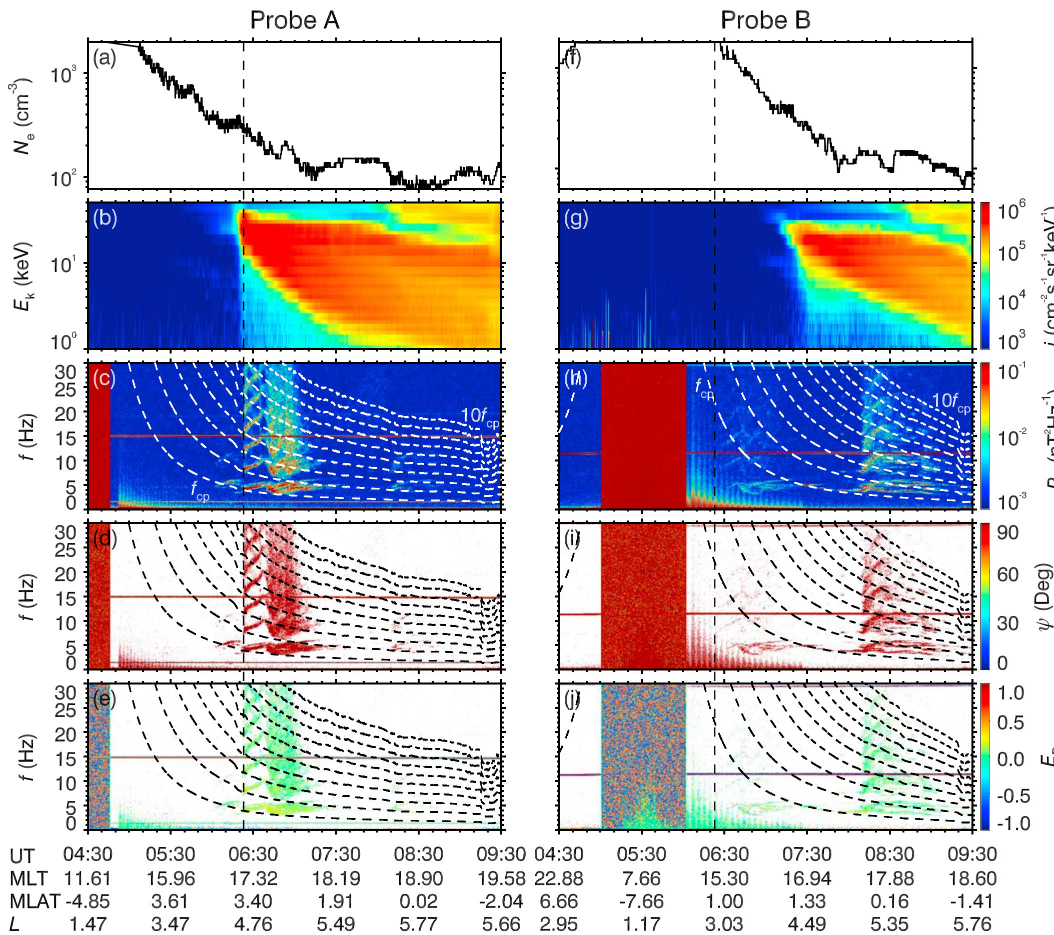

Figure 2. Generation and propagation of magnetosonic waves at frequencies below 30 Hz on 21 August 2013: (a, f) background electron density N_e, (b, g) spin-averaged proton flux j, (c, h) wave power spectral density P_B, (d, i) wave normal angle ψ, and (e, j) wave ellipticity E_B.

Figure 2. In the outer belt (Probe A), the magnetosonic emission lines starting from the first to seventh harmonics of the proton gyrofrequency can be clearly outlined following the substorm injection, supporting the local proton Bernstein mode instability theory [*Curtis and Wu*, 1979; *Boardsen et al.*, 1992; *Horne et al.*, 2000; *Gary et al.*, 2010; *Liu et al.*, 2011]. Probe A appeared to be very close to the wave source at the start of the injection. However, we cannot rule out the azimuthal shift from the source because the ambient magnetic field changes slowly in the azimuthal direction. The subsequent evolution of magnetosonic emission frequencies did not follow the variation of the harmonics of the proton gyrofrequency. Phenomenologically speaking, the magnetosonic waves reported here might be classified as the "rising tone magnetosonic waves" [*Fu et al.*, 2014; *Boardsen et al.*, 2014; *Němec et al.*, 2015]. In contrast to the previously observed rising tones with the periodic repetition at ~1–3 min [*Fu et al.*, 2014; *Boardsen et al.*, 2014; *Hospodarsky et al.*, 2016], the rising tones here lasted for a much longer time (~17 min) without any observable periodic repetitions. After 06:40 UT, the magnetosonic waves gradually became structureless at frequencies above 5 Hz. In the slot region (Probe B), the magnetosonic waves were quite weak and occurred even below the local proton gyrofrequency. In particular, these emission lines in the slot region had a rising tone feature. These observations imply once again the link between magnetosonic waves in the outer belt and in the slot region.

In Figure S1 of the supporting information, we present more details of magnetosonic waves observed by Probe A around the substorm injection. These waves are found to be quite strong with the peak-to-peak amplitude up to 6 nT and highly compressional with the ratio $P_{B\parallel}/P_B \sim 1$. They had high coherence with the planarity values close to 1, and therefore, the time series of magnetic perturbation ΔB was highly structured. The fundamental frequency oscillations were quite clear in the time series of ΔB but distorted greatly from a sinusoidal waveform.

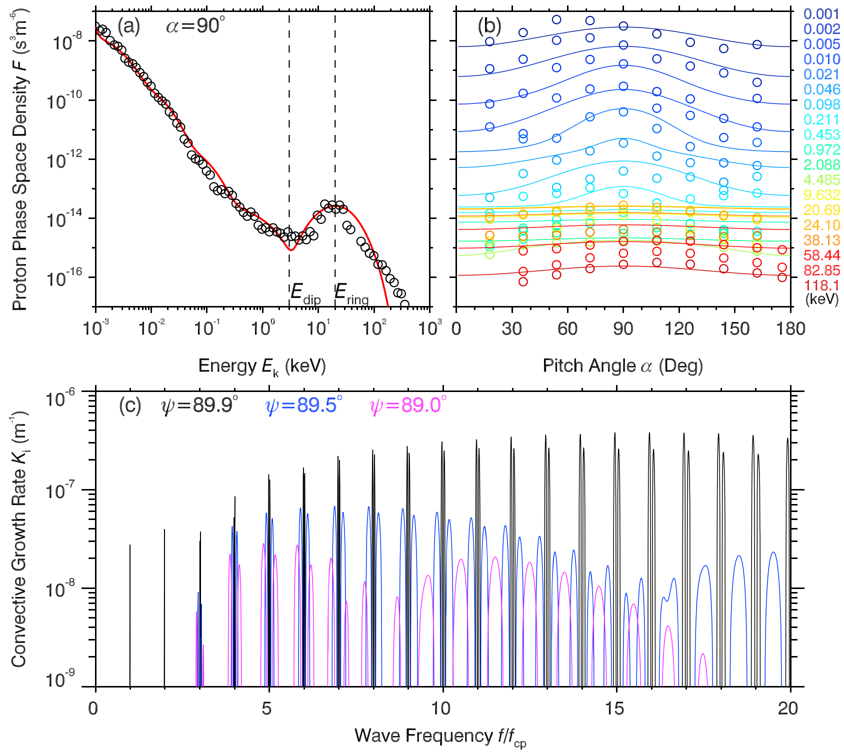

Figure 3. Magnetosonic wave instability on 21 August 2013: (a) observed (circles) and modeled (line) energy-dependent proton differential flux j at α=90°, (b) observed (circles) and modeled (lines) pitch angle-dependent proton differential flux j (color-coded according to energy), and (c) frequency-dependent wave convective growth rate K_i (color coded according to normal angle).

3.2. Wave Generation

In Figure 3, we plot the hot proton PSD profiles and the growth rates of the local proton Bernstein mode instability following the substorm injection (at 06:25 UT) within the outer radiation belt. Clearly, our model (Table 1) can well reproduce the observed proton ring with energies of ~20 keV. Based on the observations, we choose the background magnetic field B_e=260 nT and the ratio between plasma frequency and electron gyrofrequency $f_\mathrm{pe}/f_\mathrm{ce}=15$. The obtained growth rates peak near the harmonics of the proton gyrofrequency and tend to decrease with the wave normal angles decreasing. The instability frequency range is roughly consistent with the observations (Figures 1 and 2), and the peak growth rate $K_\mathrm{i}\sim 10^{-7}$ m^{-1} is comparable to the previously obtained values [*Horne et al.*, 2000]. These calculations qualitatively support the local generation of magnetosonic waves by substorm-injected protons in the outer radiation belt. However, it is found that the calculated growth rates are much smaller than the suggested threshold $K_\mathrm{i}\sim 10^{-6}$ m^{-1} [*Chen et al.*, 2010] for observable magnetosonic waves. The observed proton distribution might have been relaxed rapidly by the wave-particle interaction [*Chen et al.*, 2010], and consequently, the calculated growth rates are at a low level. In contrast to the observed dominance of wave power at the fundamental frequency (Figure S2), the calculations show weak growth or even damping of waves at the fundamental and low harmonics. The nonlinear wave-wave resonance probably contributed to the development of magnetosonic waves at the fundamental and low harmonics [*Chen et al.*, 2016].

Table 1. Fitting Parameters for Hot Proton Phase Space Density[a]

Component	n_i (m^{-3})	T_i (keV)	α_i
1	1.6000×10^{8}	8.3698×10^{-5}	1.1941
2	4.1000×10^{5}	5.2311×10^{-4}	2.8900
3	1.1000×10^{5}	2.0925×10^{-3}	4.0000
4	1.8000×10^{4}	1.8832×10^{-2}	2.7778
5	3.0000×10^{3}	3.2695×10^{-1}	1.4400
6	8.3000×10^{5}	4.4759×10^{0}	0.9785
7	-3.0000×10^{6}	7.5328×10^{0}	1.0000
8	4.8000×10^{6}	1.6949×10^{1}	1.1142

[a]Note that the seventh component with the negative density parameter is included to produce the dip of proton energy spectrum.

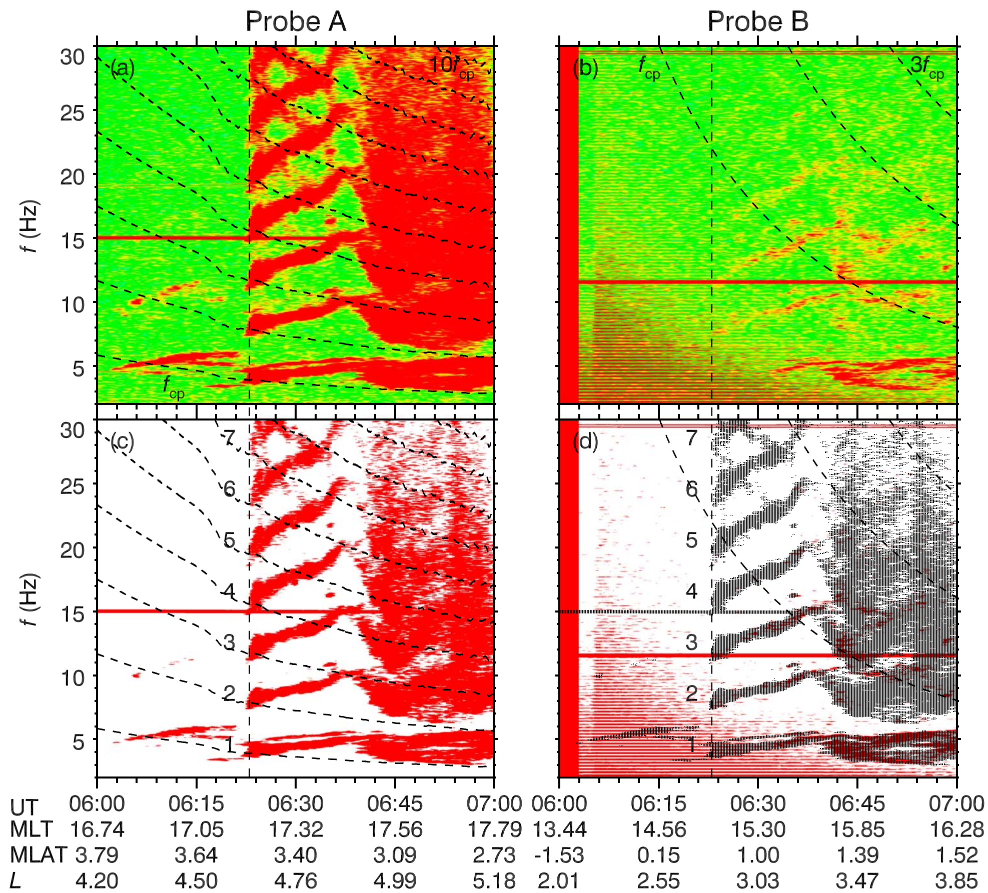

Figure 4. Comparison between magnetosonic waves observed by Van Allen Probes on 21 August 2013: (a, b) rerendered wave spectra and (c, d) isolated intense signals (red). In Figures 4c and 4d, the intensity thresholds are chosen as $P_B > 0.006$ nT^2 Hz^{-1} for Probe A and $P_B > 0.003$ nT^2 Hz^{-1} for Probe B. In Figure 4d, the overplotted gray shadows represent the intense signals of Probe A.

It should be mentioned that for this particular situation, the growth rates have some gaps at the harmonics of the proton gyrofrequency. Under the electrostatic approximation, the convective growth rate near the *n*th harmonic of the proton gyrofrequency is proportional to the following integral [*Schmidt*, 1979; *Boardsen et al.*, 1992; *Chen et al.*, 2010]:

$$K_i \propto \int_0^\infty J_n^2(x) \frac{\partial F(v_\parallel, v_\perp)}{\partial v_\perp} \mathrm{d}v_\perp, \tag{2}$$

with the *n*th-order Bessel function J_n, the argument $x = k_\perp v_\perp / \Omega_{cp}$, the proton cyclotron angular frequency $\Omega_{cp} = 2\pi f_{cp}$, and the resonant parallel velocity $v_\parallel = (\omega - n\Omega_{cp})/k_\parallel$. When $f = nf_{cp}$, the minimum resonant energy is $E_{min} \equiv \frac{1}{2} m_p v_\parallel^2 = 0$ and the integral domain covers a vast energy range $E_k < E_{dip}$ with the negative values of $\frac{\partial F}{\partial v_\perp}$. For the specific distribution in this event, the obtained growth rate happens to be negative at $f = nf_{cp}$. As the wave frequency gradually deviates from nf_{cp}, the minimum resonant energy rapidly increases. When $E_{min} > E_{ring}$, all the values of $\frac{\partial F}{\partial v_\perp}$ in the integral domain are negative. When $E_{min} = E_{dip}$, the energy range $E_{dip} < E_k < E_{ring}$ with the positive values of $\frac{\partial F}{\partial v_\perp}$ has been fully covered by the integral domain and the growth rate reaches a peak. This peak frequency tends to deviate more significantly from nf_{cp} at the smaller normal angles, since the resonant parallel velocity is inversely proportional to $k_\parallel$.

3.3. Wave Propagation

In order to evaluate the correlation between magnetosonic waves in the outer belt and in the slot region, we rerender the wave frequency-time spectra and isolate the relatively intense signals in Figure 4. Following the substorm injection, Probe A was located at $L = 4.6$ and MLT = 17.2, and Probe B was located at $L = 2.8$ and MLT = 15.1. The rising tone characteristics of the first to third magnetosonic emission lines observed by twin

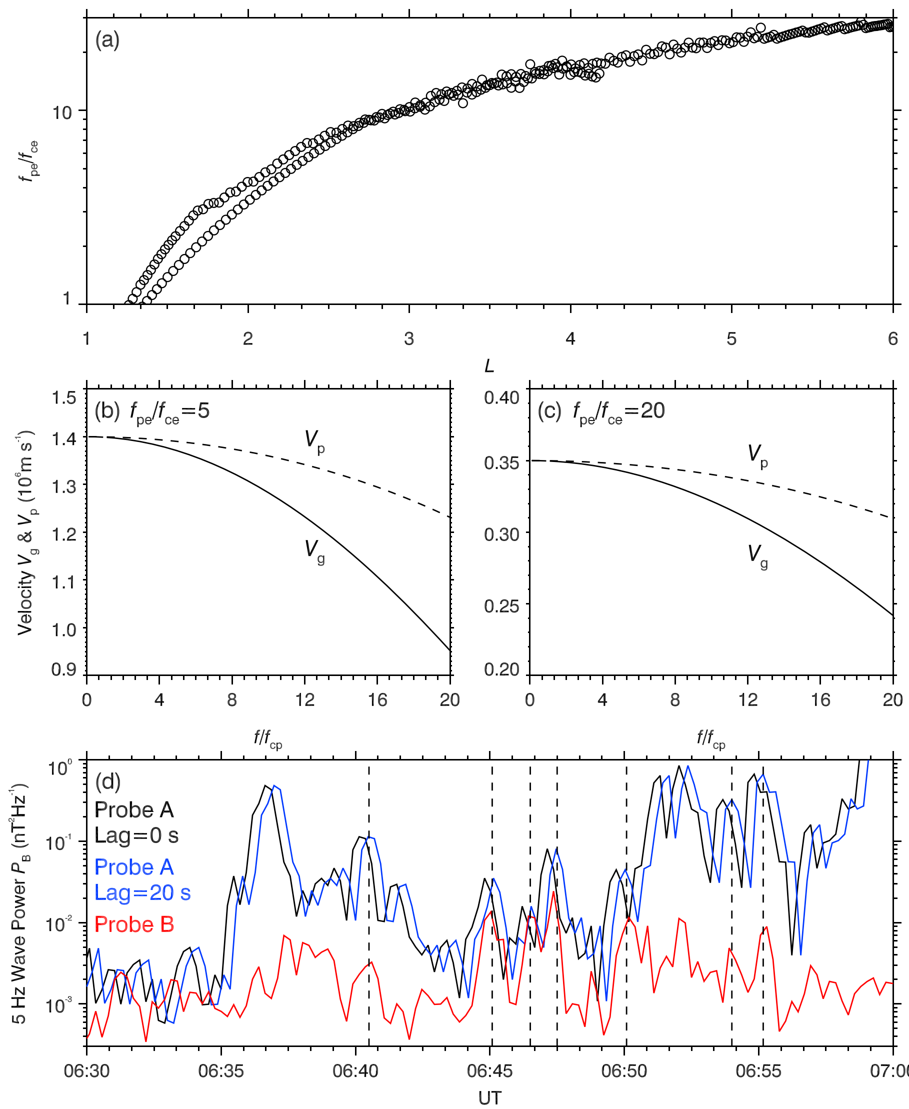

Figure 5. Estimation of time delay between wave signals received by Van Allen Probes on 21 August 2013: (a) L-dependent ratio between plasma frequency and electron gyrofrequency f_{pe}/f_{ce} observed by Probe A in the time range of 00:00–06:00 UT, (b, c) wave group V_g and phase V_p velocities under different conditions of f_{pe}/f_{ce}, and (d) 5 Hz wave power spectral densities P_B recorded by Van Allen Probes (black for Probe A without any time lag, blue for Probe A with the time lag of 20 s, and red for Probe B), with the vertical dashed lines helping identify the correlation between wave signals.

Van Allen Probes coincided with each other. At higher harmonics, the wave intensity of Probe B was too weak to allow one to identify the frequency sweeping feature. Particularly after 06:42 UT, although the twin Van Allen Probes were separated by ΔL=1.5 and by ΔMLT = 1.7, they observed the consistent oval-like structures around 5 Hz in the frequency-time spectrograms. These observations indicate that the source region of the magnetosonic waves observed by Probe B was most probably around the location of Probe A.

In Figure 5, we estimate the time delay between wave signals received by Van Allen Probes. The group and phase velocities of magnetosonic waves are calculated under the perpendicular propagation approximation (ψ=90°). At low frequencies ($f < 4f_{cp}$), the magnetosonic waves were nearly dispersionless with both group and phase velocities quite close to the local Alfvén velocity [*Boardsen et al.*, 2014], generally explaining the insignificant variation of wave frequency-time characteristics during the propagation (Figure 4). In the outer belt, the ratio between plasma frequency and electron gyrofrequency f_{pe}/f_{ce} was above 10 and the wave group velocities were in the range 250–350 km/s. In the slot region, the values of f_{pe}/f_{ce} decreased to ∼5 and the wave group velocities reached 1000–1400 km/s. The propagation time from the Probe A to Probe B was roughly 10–20 s, comparable to the time resolution of the survey-mode WFR and MAG-FFT spectra. For this event, the wave power peaked at the fundamental frequency (~5 Hz). The temporal profile of 5 Hz wave power of Probe B exhibited a similar behavior to that of Probe A with a time shift. In the time range 06:40–06:55 UT, the time delay between the wave signals of the two spacecraft is found to be approximately 20 s, generally supporting the wave propagation hypothesis.

4. Event on 19 September 2015

To illustrate the generality of the previously obtained results, we additionally show a magnetosonic wave event associated with the substorm injection on 19 September 2015 in Figures S4 and S5. In the time range of interest, both probes were located near the equator in the afternoon/dusk sector. On arrival of the substorm injection front (08:36 UT), Probe A was quite close to the plasmapause ($L=5.6$ and MLT = 16.3) and detected the prompt enhancement of magnetosonic waves below 20 Hz. The magnetosonic emissions were probably generated locally with the starting frequencies around the second to sixth harmonics of the proton gyrofrequency. These emission lines did not track the evolution of the harmonics of the proton gyrofrequency but exhibited a somewhat rising tone feature with a duration of ~23 min. This rising frequency feature in a regime with the temporal increase of the proton gyrofrequency harmonics was not quite distinct as in the case of the first event. At the third harmonic, there seem to be two emission lines starting before and after the magnetic dip (a strong diamagnetic effect associated with proton injection) [e.g., *Gurgiolo et al.*, 1979]. Note that the wave signals below f_{cp} were the electromagnetic ion cyclotron waves with the left-hand polarizations ($E_B < 0$ in Figure S4f). As shown in both WFR and MAG-FFT spectra, the magnetosonic wave enhancement of Probe B emerged at about 08:42 UT (~6 min later than that of Probe A). Such a time difference implies that no detectable wave power had been injected down to the location of Probe B in the time period 08:36–08:42 UT (probably because of the steep gradient of cold electron density near the plasmapause) [*Chen and Thorne*, 2012; *Ma et al.*, 2014]. After 08:42 UT, the rising tone characteristics of the second and third magnetosonic emission lines observed by twin Van Allen Probes agreed well with each other. Particularly in the time period of 08:55–09:20 UT, both probes observed a magnetosonic wave patch below 5 Hz with the consistent frequency sweeping rate. These observations clearly demonstrate the close relationship between magnetosonic waves of twin Van Allen Probes separated by $\Delta L=2.0$ and by ΔMLT = 4.2.

5. Conclusions and Discussions

The magnetosonic wave is a low-frequency whistler mode emission potentially contributing to the complex dynamics of Van Allen radiation belt electrons [e.g., *Horne et al.*, 2007; *Shprits*, 2009; *Bortnik and Thorne*, 2010; *Chen et al.*, 2015; *Xiao et al.*, 2015; *Li et al.*, 2016; *Yang et al.*, 2017]. It has been suggested that the magnetosonic waves are generated by the substorm-injected hot protons and can propagate over a broad spatial range [e.g., *Curtis and Wu*, 1979; *Boardsen et al.*, 1992; *Horne et al.*, 2000; *Santolík et al.*, 2002a; *Gary et al.*, 2010; *Liu et al.*, 2011; *Ma et al.*, 2014; *Santolík et al.*, 2016]. However, this theory was difficult to validate directly because of the challenging requirements on satellite locations and data processing techniques (analogous to situation about the verification of the link between chorus and hiss) [*Bortnik et al.*, 2009; *Santolik and Chum*, 2009]. In this letter, we present some experimental tests of the theory using Van Allen Probes.

At higher L shells, the substorm-injected hot protons excited the discrete magnetosonic emissions starting approximately from the harmonics of the proton gyrofrequency, qualitatively consistent with the prediction of linear proton Bernstein mode instability theory [e.g., *Curtis and Wu*, 1979; *Boardsen et al.*, 1992; *Horne et al.*, 2000; *Gary et al.*, 2010]. These emission lines exhibited a clear rising tone characteristic in the frequency-time spectrograms, implying the action of other mechanisms potentially superimposed on the linear ion Bernstein mode instability. Three plausible explanations may be given for the wave frequency rising characteristic. One possibility is the earthward movement of wave source during the substorm injection. For the event on 21 August 2013, there were ultralow frequency wave-like electric fields with a peak amplitude ~0.5 mV/m during the substorm injection (Figure S3). The shown electric field component was roughly in the radial direction, and the azimuthal electric field component approximately along the satellite spin axis was not directly measured [*Wygant et al.*, 2013]. Under the assumption of $\mathbf{E}\times\mathbf{B}$ drift alone by a −0.5 mV/m azimuthal electric field, the wave source can be transported earthward from $L=4.8$ to 4.5 within 17 min. The corresponding ambient magnetic field for the wave source will increase by $\sim(4.8/4.5)^3 = 1.21$, roughly explaining the observed increase of wave frequency. Another possibility is associated with the evolution of hot protons [*Boardsen et al.*, 2014], analogous to the situation of frequency-drifting whistlers generated by the electron cyclotron maser [*Trakhtengerts*, 1995]. At the initial state, magnetosonic waves are generated by the Bernstein mode instability at the harmonics of the proton gyrofrequency. As the magnetosonic waves diffuse the inner edge of proton ring toward lower energies, the unstable wave frequency tends to increase. For the event reported here (Figure 1b), there was a clear downward movement of the inner edge of proton ring (probably caused by the energy-dependent drift [*Lennartsson et al.*, 1979] or the magnetosonic wave-driven diffusion), potentially favoring the increase of wave frequency. A third possibility is associated with the nonlinear wave-particle interaction [*Fu et al.*, 2014], analogous to the situation of rising tone chorus generated by the nonlinear cyclotron resonance [*Omura et al.*, 2008]. However, in contrast to the previously observed rising tone magnetosonic emissions with the periodic repetition at ∼1–3 min [*Fu et al.*, 2014; *Boardsen et al.*, 2014; *Hospodarsky et al.*, 2016], the rising tones here lasted for a much longer time (15–25 min) without any observable periodic repetitions. It remains unclear whether these emissions with quite (up to 1 order of magnitude) different time durations were generated through the same physical process. In the future, both theoretical and experimental investigations are required to understand the details of the generation and evolution of all these rising tone magnetosonic waves.

At lower L shells free from substorm injection of hot protons, the magnetosonic emissions emerged nearly at the same time as those at higher L shells. These emission lines did not follow the variation of the harmonics of the proton gyrofrequency and even extended below the proton gyrofrequency. The wave signals at locations separated by ΔL up to 2.0 and by ΔMLT up to 4.2 possessed the consistent frequency-time characteristics. These observations strongly support the hypothesis about the radial and azimuthal propagation of magnetosonic waves in the Van Allen radiation belts [e.g., *Boardsen et al.*, 1992; *Horne et al.*, 2000; *Santolík et al.*, 2002a, 2016; *Ma et al.*, 2014; *Horne and Miyoshi*, 2016]. This conformation will allow further developments in the modeling of magnetosonic waves and their effects on radiation belt electrons [e.g., *Roberts and Schulz*, 1968; *Horne et al.*, 2007; *Shprits*, 2009; *Bortnik and Thorne*, 2010; *Chen et al.*, 2015; *Xiao et al.*, 2015].

Acknowledgments
We acknowledge EMFISIS, ECT, and EFW teams for the use of Van Allen Probes data. Data are available from the following websites: http://emfisis.physics.uiowa.edu/Flight/, http://www.rbsp-ect.lanl.gov/data_pub/, and http://www.space.umn.edu/rbspefw-data/. This work was supported by the National Natural Science Foundation of China grants 41631071, 41422405, 41274174, 41174125, 41131065, 41421063, 41231066, and 41304134, the Chinese Academy of Sciences grants KZCX2-EW-QN510 and KZZD-EW-01-4, the CAS Key Research Program of Frontier Sciences grant QYZDB-SSW-DQC015, the National Key Basic Research Special Foundation of China grant 2011CB811403, and the Fundamental Research Funds for the Central Universities WK2080000077.

References

Balikhin, M. A., Y. Y. Shprits, S. N. Walker, L. Chen, N. Cornilleau-Wehrlin, I. Dandouras, O. Santolik, C. Carr, K. H. Yearby, and B. Weiss (2015), Observations of discrete harmonics emerging from equatorial noise, *Nat. Commun.*, *6*, 7703, doi:10.1038/ncomms8703.

Blake, J. B., et al. (2013), The Magnetic Electron Ion Spectrometer (MagEIS) instruments aboard the Radiation Belt Storm Probes (RBSP) spacecraft, *Space Sci. Rev.*, *179*, 383–421, doi:10.1007/s11214-013-9991-8.

Boardsen, S. A., D. L. Gallagher, D. A. Gurnett, W. K. Peterson, and J. L. Green (1992), Funnel-shaped, low-frequency equatorial waves, *J. Geophys. Res.*, *97*, 14,967–14,976, doi:10.1029/92JA00827.

Boardsen, S. A., G. B. Hospodarsky, C. A. Kletzing, R. F. Pfaff, W. S. Kurth, J. R. Wygant, and E. A. MacDonald (2014), Van Allen Probe observations of periodic rising frequencies of the fast magnetosonic mode, *Geophys. Res. Lett.*, *41*, 8161–8168, doi:10.1002/2014GL062020.

Bortnik, J., and R. M. Thorne (2010), Transit time scattering of energetic electrons due to equatorially confined magnetosonic waves, *J. Geophys. Res.*, *115*, A07213, doi:10.1029/2010JA015283.

Bortnik, J., W. Li, R. M. Thorne, V. Angelopoulos, C. Cully, J. Bonnell, O. Le Contel, and A. Roux (2009), An observation linking the origin of plasmaspheric hiss to discrete chorus emissions, *Science*, *324*, 775–778, doi:10.1126/science.1171273.

Chen, L., and R. M. Thorne (2012), Perpendicular propagation of magnetosonic waves, *Geophys. Res. Lett.*, *39*, L14102, doi:10.1029/2012GL052485.

Chen, L., R. M. Thorne, V. K. Jordanova, and R. B. Horne (2010), Global simulation of magnetosonic wave instability in the storm time magnetosphere, *J. Geophys. Res.*, *115*, A11222, doi:10.1029/2010JA015707.

Chen, L., A. Maldonado, J. Bortnik, R. M. Thorne, J. Li, L. Dai, and X. Zhan (2015), Nonlinear bounce resonances between magnetosonic waves and equatorially mirroring electrons, *J. Geophys. Res. Space Physics*, *120*, 6514–6527, doi:10.1002/2015JA021174.

Chen, L., J. Sun, Q. Lu, X. Gao, Z. Xia, and Z. Zhima (2016), Generation of magnetosonic waves over a continuous spectrum, *J. Geophys. Res. Space Physics*, *121*, 1137–1147, doi:10.1002/2015JA022089.

Curtis, S. A., and C. S. Wu (1979), Gyroharmonic emissions induced by energetic ions in the equatorial plasmasphere, *J. Geophys. Res.*, *84*, 2597–2607, doi:10.1029/JA084iA06p02597.

Fu, H. S., J. B. Cao, Z. Zhima, Y. V. Khotyaintsev, V. Angelopoulos, O. Santolík, Y. Omura, U. Taubenschuss, L. Chen, and S. Y. Huang (2014), First observation of rising-tone magnetosonic waves, *Geophys. Res. Lett.*, *41*, 7419–7426, doi:10.1002/2014GL061867.

Funsten, H. O., et al. (2013), Helium, Oxygen, Proton, and Electron (HOPE) mass spectrometer for the Radiation Belt Storm Probes mission, *Space Sci. Rev.*, *179*, 423–484, doi:10.1007/s11214-013-9968-7.

Gary, S. P., K. Liu, D. Winske, and R. E. Denton (2010), Ion Bernstein instability in the terrestrial magnetosphere: Linear dispersion theory, *J. Geophys. Res.*, *115*, A12209, doi:10.1029/2010JA015965.

Gulelmi, A. V., B. I. Klaine, and A. S. Potapov (1975), Excitation of magnetosonic waves with discrete spectrum in the equatorial vicinity of the plasmapause, *Planet. Space Sci.*, *23*, 279–286, doi:10.1016/0032-0633(75)90133-6.

Gurgiolo, C., C. S. Lin, B. Mauk, G. K. Parks, and C. McIlwain (1979), Plasma injection and diamagnetism, *J. Geophys. Res.*, *84*, 2049–2056, doi:10.1029/JA084iA05p02049.

Gurnett, D. A. (1976), Plasma wave interactions with energetic ions near the magnetic equator, *J. Geophys. Res.*, *81*, 2765–2770, doi:10.1029/JA081i016p02765.

Horne, R. B. (1989), Path-integrated growth of electrostatic waves: The generation of terrestrial myriametric radiation, *J. Geophys. Res.*, *94*, 8895, doi:10.1029/JA094iA07p08895.

Horne, R. B., and Y. Miyoshi (2016), Propagation and linear mode conversion of magnetosonic and electromagnetic ion cyclotron waves in the radiation belts, *Geophys. Res. Lett.*, *43*, 10,034–10,039, doi:10.1002/2016GL070216.

Horne, R. B., G. V. Wheeler, and H. S. C. K. Alleyne (2000), Proton and electron heating by radially propagating fast magnetosonic waves, *J. Geophys. Res.*, *105*, 27,597–27,610, doi:10.1029/2000JA000018.

Horne, R. B., R. M. Thorne, S. A. Glauert, N. P. Meredith, D. Pokhotelov, and O. Santolík (2007), Electron acceleration in the Van Allen radiation belts by fast magnetosonic waves, *Geophys. Res. Lett.*, *34*, L17107, doi:10.1029/2007GL030267.

Hospodarsky, G. B., W. S. Kurth, C. A. Kletzing, S. R. Bounds, O. Santolík, R. M. Thorne, W. Li, T. F. Averkamp, J. R. Wygant, and J. W. Bonnell (2016), Plasma wave measurements from the Van Allen Probes, in *Magnetosphere-Ionosphere Coupling in the Solar System*, edited by C. R. Chappell et al., pp. 127–143, John Wiley, Hoboken, N. J., doi:10.1002/9781119066880.ch10.

Hrbáčková, Z., O. Santolík, F. Němec, E. E. Macúšová, and N. Cornilleau-Wehrlin (2015), Systematic analysis of occurrence of equatorial noise emissions using 10 years of data from the Cluster mission, *J. Geophys. Res. Space Physics*, *120*, 1007–1021, doi:10.1002/2014JA020268.

Kasahara, Y., H. Kenmochi, and I. Kimura (1994), Propagation characteristics of the ELF emissions observed by the satellite Akebono in the magnetic equatorial region, *Radio Sci.*, *29*, 751–767, doi:10.1029/94RS00445.

Kletzing, C. A., et al. (2013), The Electric and Magnetic Field Instrument Suite and Integrated Science (EMFISIS) on RBSP, *Space Sci. Rev.*, *179*, 127–181, doi:10.1007/s11214-013-9993-6.

Kurth, W. S., S. D. Pascuale, J. B. Faden, C. A. Kletzing, G. B. Hospodarsky, S. Thaller, and J. R. Wygant (2014), Electron densities inferred from plasma wave spectra obtained by the waves instrument on Van Allen Probes, *J. Geophys. Res. Space Physics*, *120*, 904–914, doi:10.1002/2014JA020857.

Lennartsson, W., E. G. Shelley, R. D. Sharp, R. G. Johnson, and H. Balsiger (1979), Some initial ISEE-1 results on the ring current composition and dynamics during the magnetics storm of December 11, 1977, *Geophys. Res. Lett.*, *6*, 483–486, doi:10.1029/GL006i006p00483.

Li, J., et al. (2016), Formation of energetic electron butterfly distributions by magnetosonic waves via Landau resonance, *Geophys. Res. Lett.*, *43*, 3009–3016, doi:10.1002/2016GL067853.

Liu, K., S. P. Gary, and D. Winske (2011), Excitation of magnetosonic waves in the terrestrial magnetosphere: Particle-in-cell simulations, *J. Geophys. Res.*, *116*, A07212, doi:10.1029/2010JA016372.

Ma, Q., W. Li, R. M. Thorne, and V. Angelopoulos (2013), Global distribution of equatorial magnetosonic waves observed by THEMIS, *Geophys. Res. Lett.*, *40*, 1895–1901, doi:10.1002/grl.50434.

Ma, Q., W. Li, L. Chen, R. M. Thorne, C. A. Kletzing, W. S. Kurth, G. B. Hospodarsky, G. D. Reeves, M. G. Henderson, and H. E. Spence (2014), The trapping of equatorial magnetosonic waves in the Earth's outer plasmasphere, *Geophys. Res. Lett.*, *41*, 6307–6313, doi:10.1002/2014GL061414.

Mauk, B. H., N. J. Fox, S. G. Kanekal, R. L. Kessel, D. G. Sibeck, and A. Ukhorskiy (2013), Science Objectives and Rationale for the Radiation Belt Storm Probes Mission, *Space Sci. Rev.*, *179*, 3–27, doi:10.1007/s11214-012-9908-y.

Meredith, N. P., R. B. Horne, and R. R. Anderson (2008), Survey of magnetosonic waves and proton ring distributions in the Earth's inner magnetosphere, *J. Geophys. Res.*, *113*, A06213, doi:10.1029/2007JA012975.

Němec, F., O. Santolík, K. Gereová, E. Macúšová, Y. de Conchy, and N. Cornilleau-Wehrlin (2005), Initial results of a survey of equatorial noise emissions observed by the Cluster spacecraft, *Planet. Space Sci.*, *53*, 291–298, doi:10.1016/j.pss.2004.09.055.

Němec, F., O. Santolík, Z. Hrbáčková, J. S. Pickett, and N. Cornilleau-Wehrlin (2015), Equatorial noise emissions with quasiperiodic modulation of wave intensity, *J. Geophys. Res. Space Physics*, *120*, 2649–2661, doi:10.1002/2014JA020816.

Omura, Y., Y. Katoh, and D. Summers (2008), Theory and simulation of the generation of whistler-mode chorus, *J. Geophys. Res.*, *113*, A04223, doi:10.1029/2007JA012622.

Perraut, S., A. Roux, P. Robert, R. Gendrin, J.-A. Sauvaud, J.-M. Bosqued, G. Kremser, and A. Korth (1982), A systematic study of ULF waves above F_{H+} from GEOS 1 and 2 measurements and their relationships with proton ring distributions, *J. Geophys. Res.*, *87*, 6219–6236, doi:10.1029/JA087iA08p06219.

Roberts, C. S., and M. Schulz (1968), Bounce resonant scattering of particles trapped in the Earth's magnetic field, *J. Geophys. Res.*, *73*, 7361–7376, doi:10.1029/JA073i023p07361.

Russell, C. T., R. E. Holzer, and E. J. Smith (1970), OGO 3 observations of ELF noise in the magnetosphere. 2. The nature of the equatorial noise, *J. Geophys. Res.*, *75*, 755–768, doi:10.1029/JA075i004p00755.

Santolik, O., and J. Chum (2009), The origin of plasmaspheric hiss, *Science*, *324*, 729–730, doi:10.1126/science.1172878.

Santolík, O., J. S. Pickett, D. A. Gurnett, M. Maksimovic, and N. Cornilleau-Wehrlin (2002a), Spatiotemporal variability and propagation of equatorial noise observed by Cluster, *J. Geophys. Res.*, *107*(A12), 1495, doi:10.1029/2001JA009159.

Santolík, O., J. S. Pickett, D. A. Gurnett, and L. R. O. Storey (2002b), Magnetic component of narrowband ion cyclotron waves in the auroral zone, *J. Geophys. Res. Space Physics*, *107*(A12), 1444, doi:10.1029/2001JA000146.

Santolík, O., M. Parrot, and F. Lefeuvre (2003), Singular value decomposition methods for wave propagation analysis, *Radio Sci.*, *38*(1), 1010, doi:10.1029/2000RS002523.

Santolík, O., J. S. Pickett, D. A. Gurnett, J. D. Menietti, B. T. Tsurutani, and O. Verkhoglyadova (2010), Survey of Poynting flux of whistler mode chorus in the outer zone, *J. Geophys. Res.*, *115*, A00F13, doi:10.1029/2009JA014925.

Santolík, O., M. Parrot, and F. Němec (2016), Propagation of equatorial noise to low altitudes: Decoupling from the magnetosonic mode, *Geophys. Res. Lett.*, *43*, 6694–6704, doi:10.1002/2016GL069582.

Schmidt, G. (1979), *Physics of High Temperature Plasmas*, Academic Press, New York.

Shprits, Y. Y. (2009), Potential waves for pitch-angle scattering of near-equatorially mirroring energetic electrons due to the violation of the second adiabatic invariant, *Geophys. Res. Lett.*, *36*, L12106, doi:10.1029/2009GL038322.

Shprits, Y. Y., A. Runov, and B. Ni (2013), Gyro-resonant scattering of radiation belt electrons during the solar minimum by fast magnetosonic waves, *J. Geophys. Res. Space Physics*, *118*, 648–652, doi:10.1002/jgra.50108.

Spence, H. E., et al. (2013), Science goals and overview of the Energetic Particle, Composition, and Thermal Plasma (ECT) Suite on NASA's Radiation Belt Storm Probes (RBSP) mission, *Space Sci. Rev.*, *179*, 311–336, doi:10.1007/s11214-013-0007-5.

Trakhtengerts, V. Y. (1995), Magnetosphere cyclotron maser: Backward wave oscillator generation regime, *J. Geophys. Res.*, *100*, 17,205–17,210, doi:10.1029/95JA00843.

Tsurutani, B. T., B. J. Falkowski, J. S. Pickett, O. P. Verkhoglyadova, O. Santolik, and G. S. Lakhina (2014), Extremely intense ELF magnetosonic waves: A survey of polar observations, *J. Geophys. Res. Space Physics*, *119*, 964–977, doi:10.1002/2013JA019284.

Tsyganenko, N. A., and M. I. Sitnov (2005), Modeling the dynamics of the inner magnetosphere during strong geomagnetic storms, *J. Geophys. Res.*, *110*, A03208, doi:10.1029/2004JA010798.

Wygant, J., et al. (2013), The electric field and waves instruments on the Radiation Belt Storm Probes mission, *Space Sci. Rev.*, *179*(1–4), 183–220, doi:10.1007/s11214-013-0013-7.

Xiao, F., C. Yang, Z. Su, Q. Zhou, Z. He, Y. He, D. Baker, H. Spence, H. Funsten, and J. Blake (2015), Wave-driven butterfly distribution of Van Allen belt relativistic electrons, *Nat. Commun.*, *6*, 8590, doi:10.1038/ncomms9590.

Yang, C., et al. (2017), A positive correlation between energetic electron butterfly distributions and magnetosonic waves in the radiation belt slot region, *Geophys. Res. Lett.*, *44*, 3980–3990, doi:10.1002/2017GL073116.

Zhao, H., X. Li, J. B. Blake, J. F. Fennell, S. G. Claudepierre, D. N. Baker, A. N. Jaynes, D. M. Malaspina, and S. G. Kanekal (2014), Peculiar pitch angle distribution of relativistic electrons in the inner radiation belt and slot region, *Geophys. Res. Lett.*, *41*, 2250–2257, doi:10.1002/2014GL059725.